

A minimal neuronal model for synaptic integration

Adrian Alva* and Harjinder Singh†

Center for Computational Natural Sciences and Bioinformatics, IIIT Hyderabad, India

(Dated: December 11, 2020)

The Fitzhugh-Nagumo system is a prototypical model for simulating different modes of neuronal spiking activity. We introduce a minimal model for synaptic integration of action potentials and explore the basic properties of postsynaptic neurons thus defined. Our model supports two basic modes of summation that resemble the biological scenario. We compare presynaptic and postsynaptic neurons for basic noise enhancing properties such as stochastic resonance, coherence resonance and firing rate statistics. The model can be used to investigate the response of postsynaptic neurons to different kinds of synaptic stimulation, especially in those cases where differences in synaptic connectivity are known to confer a significant functional advantage.

I. INTRODUCTION

The Fitzhugh-Nagumo (FN) model is a system of ordinary differential equations that has been used to simulate the dynamics of biological excitable systems such as neurons. The model was originally written down as a simplification of the classic Hodgkin-Huxley (HH) equations [1] which describe action potential propagation in axons. The reduction of the 4-dimensional HH equations to the 2-dimensional FN system makes it especially convenient to describe and analyse distinct modes of behaviour on a phase plane. As a qualitative model of excitability, the FN system is capable of simulating various dynamical modes of neurons such as action potentials, graded potentials, continuous spiking, mixed mode oscillations, etc. The FN model is also of theoretical interest as an example of a singularly perturbed system and has been investigated for the presence of canard orbits. Though not as detailed as the HH equations, it serves as a reasonably good phenomenological model to investigate the geometry of different kinds of trajectories.

Neurons are inherently noisy and the functional role of a variety of stochastic fluctuations in inter-spike variability has been documented [2–4]. The FN model has been shown to account for several noise driven phenomena such as stochastic resonance [5–7], coherence resonance [8], resonant activation and noise enhanced stability [9]. Multiple stochastic FN neurons can be coupled to produce noise-induced synchronization [10] and phase locking [11]. In this paper, we numerically investigate a basic extension of the FN model to describe the integration of excitatory synaptic potentials. We first motivate the rationale behind the model by describing the properties of the excitation threshold for FN neurons. Then it is shown that the model supports two kinds of summation for synaptic stimuli that resemble the experimentally observed types. Next, the postsynaptic neurons in our model are investigated for noise enhanced properties such as stochastic resonance and coherence resonance.

We then summarize our findings and highlight certain limitations and possible improvements. Finally, some important questions and points of further inquiry are listed.

II. EXCITATION THRESHOLD IN THE FN MODEL

The FN equations consist of two state variables whose dynamics operates on significantly different timescales (as is the case for all singularly perturbed systems). The fast "voltage" variable (v) mimics a neuron's membrane potential and is complemented by a slow "recovery" variable (w). The dynamical equations are given by:

$$\epsilon \dot{v} = v(v - a)(1 - v) - w + I(t) \quad (1)$$

$$\dot{w} = v - w - b \quad (2)$$

where the parameters a and b have values 0.5 and 0.15 respectively and ϵ represents the ratio of the two timescales and is typically set to 0.005. A time dependent current injection into the neuron is modelled by the function I . In contrast to the all-or-none nature of neuronal firing patterns, the FN model does not exhibit a well defined threshold for excitability [12, 13]. That is to say, action potentials with a range of amplitudes are possible depending on the choice of the current term $I(t)$. However, there is a sense in which one can approximate a firing threshold in the FN model and this requires the analysis of a family of trajectories known as *canards* [14–17]. The current term I serves as a bifurcation parameter that delineates the different regimes of neuronal firing. Choices of I that lead to the w -nullcline intersecting the cubic v -nullcline on either the left or right branch give rise to stable and unstable nodes respectively. An intersection on the middle branch of the v -nullcline on the other hand gives rise to stable limit cycles which mimics tonic firing or bursting of biological neurons. For the former case when the intersection lies on the left branch, an appropriate initial condition can generate a single excitation that manifests as an excursion around the cubic nullcline that returns back to the fixed point. Alternatively, we can set the initial condition to be the location of the fixed

* adrianjoseph.alva@research.iiit.ac.in

† laltu@iiit.ac.in

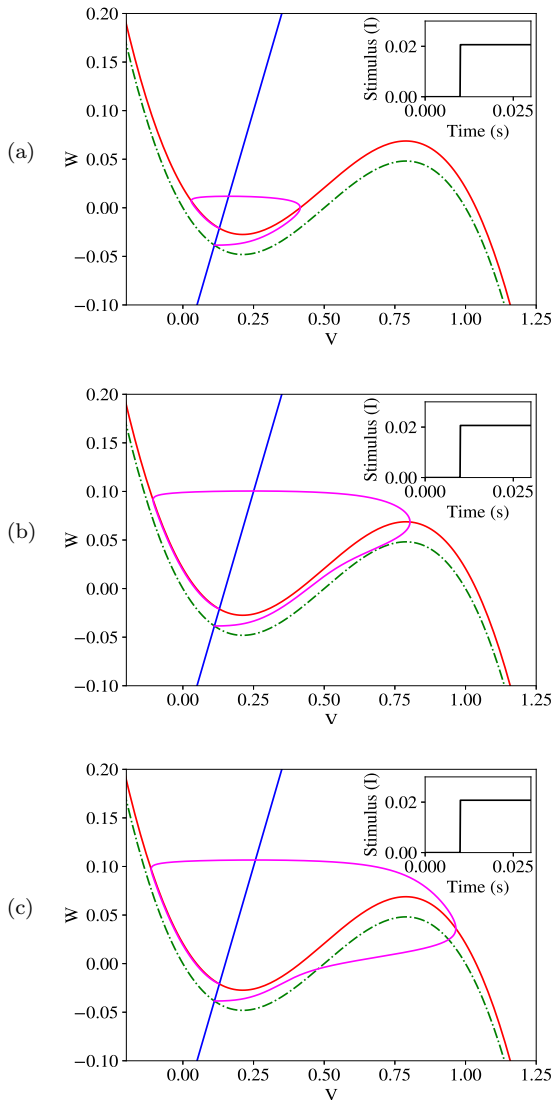


FIG. 1: (a) A small amplitude excursion corresponding to an instantaneous current injection at $t = 0.01s$ ($I = 0.02063$) (b) An excursion in the canard regime approximating a maximal canard ($I = 0.0206472$) (c) A large amplitude excursion ($I = 0.02075$). The green (dotted) and red cubics represent the nullclines before and after the current stimulus (inset) respectively. The trajectories were obtained by numerically integrating equations 1 and 2 using an Euler scheme with time step 0.0001.

point when $I = 0$ and supply an instantaneous current injection at a specified time (by setting I to some small positive value). This would correspond to the cubic nullcline instantaneously shifting upwards which would send the initial condition point on an excursion that ends up on the new fixed point (Fig. 1).

However, the amplitude of this excitation can vary over a large range depending on the amount by which we shift the nullcline upwards (i.e. the value of the instantaneous current injection I). Moreover, the transition from small

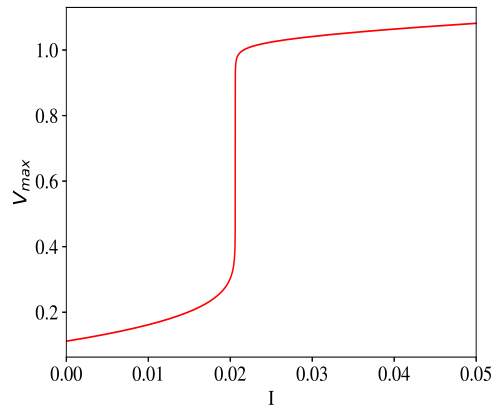


FIG. 2: A canard explosion within the parameter range $I \in (0.2063, 0.2066)$. Despite the absence of a rigid firing threshold, the canard explosion allows us to posit a firing manifold for the FN system.

amplitude excitations to large amplitude excitations occurs in an exponentially small ($O(e^{-\epsilon})$) region of the parameter range I . Within this range, trajectories known as canards track the middle branch of the cubic nullcline for a relatively long ($O(\frac{1}{\epsilon})$) time (Fig. 1b). The middle branch of the cubic nullcline is called the *repelling slow manifold* since nearby trajectories diverge sharply from it. The right and left branches in contrast are the *attracting slow manifolds* since nearby trajectories converge onto them. Informally, canards are trajectories that follow both the attracting and repelling branches of the slow manifold for a considerable amount of time [15]. The canard phenomenon in the FN model has been analysed in the vicinity of a supercritical Hopf bifurcation when the intersection of the nullclines crosses the local minima of the left cubic branch. Beyond this point, in an exponentially small region of the parameter (I) range, small amplitude (stable) limit cycles exist which then transition abruptly into large amplitude (stable) limit cycles. The abrupt transition is called a *canard explosion*. In this paper, we set the nullcline intersection point on the left branch away from the bifurcation point.

We are concerned with the dynamics of the FN system when it is subjected to step-like stimuli (a sum of heaviside functions). By increasing the height of the instantaneous step stimulus, a canard transition occurs in a small region of the parameter space which is shown in Fig. 2. Here, we plot the maximum value of v (amplitude of excitation) against the stimulus strength I . Consequently, I is also called the canard parameter and allows us to define an excitation manifold for the FN system. That is to say, we can treat all values of I below the canard regime as "subthreshold" and all values above it as "suprathreshold" since the corresponding trajectories undergo small and large amplitude excitations respectively after the step stimulus has been applied.

III. NOISY FN MODEL FOR SYNAPTIC INPUT

Synaptic integration of information primarily exhibits two modes known as spatial and temporal summation [18–20]. We devise a minimal model for summation of post-synaptic action potentials via a chemical synapse. Neurotransmitter induced post-synaptic potentials can overlap in the cell body (axon hillock) of the post-synaptic neuron within a brief window of time (set by the diffusion rate of ions) to depolarize the axon and generate an action potential. However, many of these summation events are subthreshold and cause small amplitude *graded* potentials.

We assume that a presynaptic neuron's voltage crossing a threshold value $v_T = 0.8$ generates a (neurotransmitter mediated) step stimulus that is fed into the current term $I(t)$ of the post-synaptic neuron. The step stimulus is modelled by a heaviside function $H(v - v_T)$. The dynamical equation (1) is then modified as follows. Equation (2) remains unchanged.

$$\epsilon \dot{v} = v(v - a)(1 - v) - w + I(t) + \sigma \xi(t) \quad (3)$$

where σ is the standard deviation of the noise term $\xi(t)$ modelled by a normalized Wiener process with autocorrelation $\langle \xi(t)\xi(t') \rangle = \sigma^2 \delta(t - t')$. To investigate the synchronization properties of the synapse, we assign a sinusoidal term to the current for presynaptic neurons, i.e.

$$I(t) = A \sin(2\pi ft + \phi) \quad (4)$$

where A is a subthreshold signal (unable to cause excitations beyond v_T) and ϕ is a random phase sampled from the Gaussian distribution with $\mu = 0$ and $\sigma = \pi/4$. Unlike step stimuli, for a sinusoidal stimulus there exists an amplitude (A) versus frequency (f) parameter plane which defines a sharp threshold curve for excitability (as opposed to an excitation *manifold* for step stimuli) [9]. For the postsynaptic neuron, we define the input current function as the sum of N heaviside functions from N presynaptic neurons, with an appropriate coefficient to represent a mean-field like coupling:

$$I(t) = \frac{I_T}{N_{\min}} \sum_{i=1}^N H(v_i - v_T) \quad (5)$$

The threshold I_T is chosen from Fig. 2 as a value with sufficient gap from the canard explosion. The parameter N_{\min} represents the minimum number of presynaptic firings required to sum and generate a post-synaptic action potential. If step stimuli from N_{\min} neurons were to overlap simultaneously, $I(t)$ in equation (5) would equal the firing threshold I_T . We note here that N_{\min} need not be strictly an integer and that the coupling can be tuned continuously by setting it to any arbitrary value. Because there is always a time gap between successive summation events, the trajectory drifts for a while until the next stimulus in the sequence. This time gap must be small enough to prevent the net drift from falling into

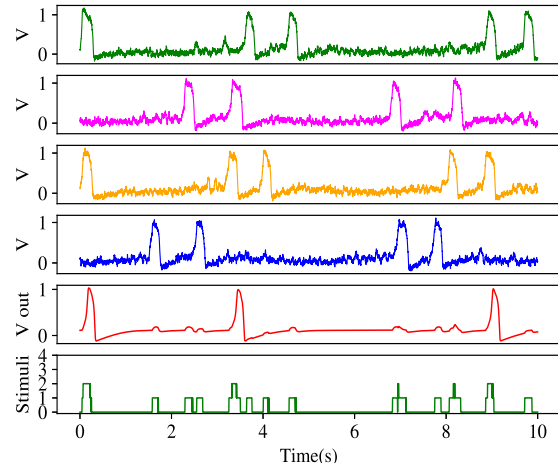


FIG. 3: Voltage trajectories for $N = 4$ presynaptic neurons and a postsynaptic neuron for which $N_{\min}=2$. The driving frequency for all presynaptic neurons is set at $f = 0.2Hz$ and subthreshold amplitude at $A = 0.07$. The standard deviation of noise for all presynaptic neurons, $\sigma = 0.003$. The initial condition is set as $v_0 = 0.1115$, $w_0 = -0.0385$ which is the point of intersection of the nullclines when no current stimulus is applied ($I = 0$). The postsynaptic neuron is noiseless for this simulation to avoid noise induced excitations. Step stimuli from presynaptic firings (green) cause the post-synaptic neuron (red) to depolarise under appropriate conditions of stimulus height and width. The two suprathreshold stimuli between $t = 6s$ and $t = 9s$ do not cause excitations due to insufficient width and instead result in graded potentials.

or below the canard region of the nullcline defined by the composite step.

To integrate equations (2) and (3), we use a standard Euler-Maruyama scheme [21, 22]. The stochastic differential equations corresponding to equations (3) and (2) respectively are:

$$dv = \frac{1}{\epsilon} [v(v - a)(1 - v) - w + I]dt + \frac{\sigma}{\epsilon} dW \quad (6)$$

$$dw = (v - w - b)dt \quad (7)$$

The Euler-Maruyama scheme corresponding to equations (6) and (7) is therefore:

$$v_{n+1} = v_n + \frac{1}{\epsilon} [v_n(v_n - a)(1 - v_n) - w_n + I]\delta t + \frac{\sigma}{\epsilon} \sqrt{\delta t} \Delta W_n \quad (8)$$

$$w_{n+1} = w_n + (v_n - w_n - b)\delta t \quad (9)$$

where ΔW_n is sampled from a Gaussian distribution with unit variance. For all simulations that follow, we choose a step size $\delta t = 0.001$ and a firing threshold $I_T = 0.027$. Sample trajectories for $N = 4$ presynaptic neurons are

shown in Fig. 3. The minimal model for synaptic integration in equation (5) supports two modes of summation. For our choice of parameters, the typical duration for which a presynaptic action potential remains above the threshold v_T is approximately between 0.1s and 0.15s. Consequently, if the summation of two or more stimuli exceeds the postsynaptic firing threshold I_T , an action potential is generated (spatial summation) provided the width of time for which the summed stimulus persists is sufficient within the duration of the first step stimulus. In Figs. 4(a) and 4(b), we show a spatial summation of two step stimuli of height $I_T/2$ each resulting in either a graded potential or an action potential depending on the width of the net stimulus. If the width of the net stimulus is insufficient for spatial summation, an action potential can still be generated if two or more suprathreshold stimuli follow in quick succession (temporal summation). This is because the time between two successive stimuli is small enough compared to the time scale at which the trajectory approaches the fixed point. In other words, the voltage "lost" by the drift between two quickly succeeding suprathreshold stimuli is negligible. We note here that this kind of summation is not equivalent to the temporal summation observed in biological neurons. There, while stimuli with high frequency are required akin to our model, each individual stimulus can still be subthreshold. In our model, temporal summation works only for high frequency suprathreshold stimuli where each stimulus itself may not generate an action potential. In Figs. 4(c) and 4(d), we show two successive stimuli resulting in either a graded potential or an action potential via temporal summation.

IV. NOISE INDUCED SYNCHRONIZATION

A classic result in the theory of stochastic processes is that noise can increase the synchronization of the response of certain nonlinear systems to an external periodic signal. The general effect is termed stochastic resonance (SR) [23, 24]. The simplest system which can be shown to exhibit SR is an overdamped Brownian particle in a double well potential. Modulating the potential with a weak periodic signal alternatively raises and lowers the two wells, although the signal by itself is insufficient to cause inter-well transitions. Adding white noise to the external forcing however, can result in the particle switching wells. Intuitively, this phenomenon is understood as the result of a time-scale matching condition [23]: the average waiting/residence time of the particle between transitions is comparable with half the period of the driving signal. Consequently, for a given value of the driving signal's frequency, there exists a corresponding noise intensity that achieves the highest tuning between noise induced transitions and the driving signal.

SR has been documented extensively in experimental systems including sensory neurons [25, 26]. Moreover, interspike interval histograms from recordings of neural

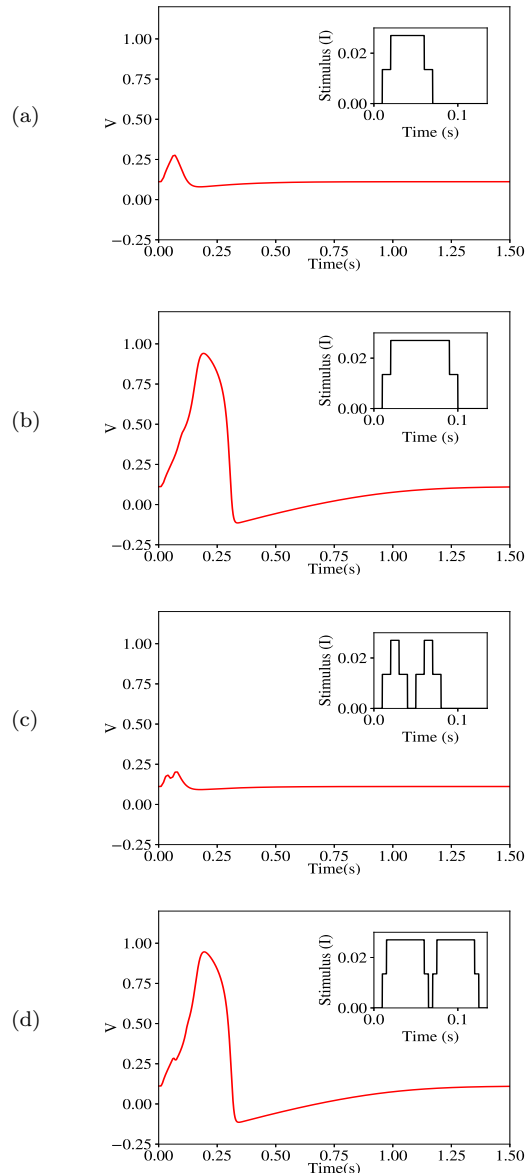


FIG. 4: Spatial and temporal summation of step stimuli (insets). (a) Graded potential generated by a spatially summed stimulus of width 0.04s (b) Action potential generated by a spatially summed stimulus of width 0.07s (c) Graded potential for temporally summed stimuli each having width 0.01s (d) Action potential for temporally summed stimuli each having width 0.045s.

activity have been shown to resemble the residence-time distributions of a sinusoidally driven bistable potential with additive noise [5]. Subsequently, SR has been numerically shown in several neuronal models. For the FN system, the SR effect can be analytically derived by casting the original dynamical equation for voltage (3) into a form equivalent to Langevin dynamics in a one-dimensional double well potential [6]. This approximation works essentially due to the large separation of

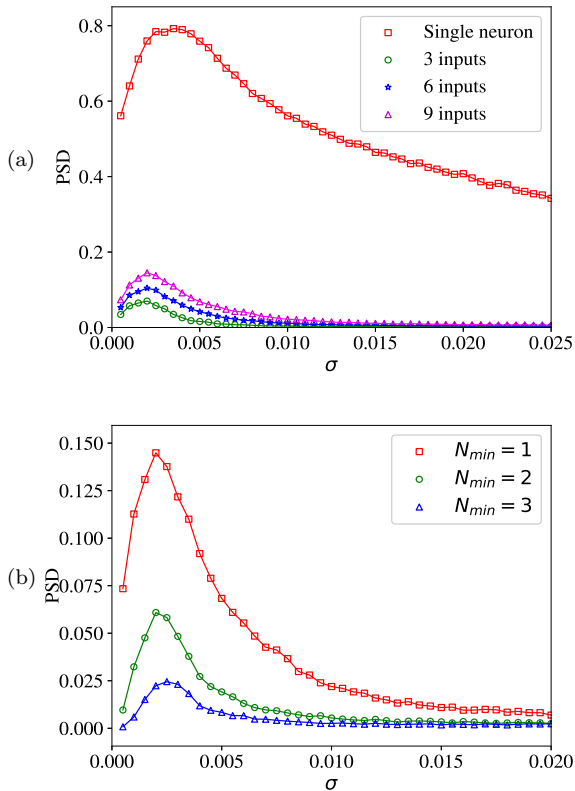


FIG. 5: (a) Response amplitudes for different values of N plotted as a function of standard deviation of noise contrasted with a single presynaptic neuron (red). The parameter $N_{\min} = 1$ for all 3 cases. The power spectral densities from the periodogram were averaged over 100 trajectories (each run for 100s). (b) Response amplitudes for different values of N_{\min} for a post-synaptic neuron with 9 inputs. Again, the values of power spectral densities were averaged over 100 trajectories each run for 100s. The driving signal for both (a) and (b) was setup with subthreshold amplitude $A = 0.07$ and frequency $f = 0.2Hz$.

time-scales set by $\epsilon \ll 1$ so that $\dot{w} \sim 0$ on the fast (nearly straight line) branch of the excursion along v . A noise induced "escape" from the fixed point is analogous to a switching between wells. The trajectory returns to the fixed point from the other well via a different degree of freedom (w) [6]. The simplest measure characterising SR is the power spectral density $S_{\sigma}(f)$ of the spike train (v) computed at the driving frequency f and for a given standard deviation σ of the additive white noise $\xi(t)$. We use a periodogram to estimate the power spectral density of the voltage. In Fig. 5, we show comparisons between a single FN neuron and a post-synaptic FN neuron with different numbers of presynaptic inputs. For a single neuron directly stimulated by a sinusoidal input current, $S_{\sigma}(f)$ is significantly higher than the post-synaptic neuron (Fig. 5a) since the subthreshold (sinusoidal) oscillation has a major contribution to $S_{\sigma}(f)$. Postsynaptic neurons on the other hand are stimulated purely by step

stimuli from the synapses. Thus $S_{\sigma}(f)$ for the postsynaptic response is contributed almost entirely by firings entrained by the step stimuli which is why the power spectral density is lower compared to the presynaptic case. For low values of noise intensity, while each individual presynaptic neuron has a low probability of firing, the probability of *some* presynaptic neuron firing is scaled up depending on N . That is, for the same noise intensity, while each presynaptic neuron may not fire on a signal crest, the postsynaptic neuron does with high likelihood due to inputs from many independent synapses. In addition, the post-synaptic neuron also exhibits random noise induced firings (when $I(t) = 0$). The combined effect is that the peak of the power spectral density in Fig. 5(a) shifts slightly to the left in contrast to the peak corresponding to the presynaptic neuron. We also performed the same simulation for a noiseless postsynaptic neuron and the resulting PSD curves had the same height except for a much slower decrease following the peak. Fig 5(b) shows the power spectral densities of a postsynaptic neuron with different values for the minimum number of synaptic excitations (N_{\min}) required to elicit firing. As expected, increasing the synaptic coupling (by decreasing N_{\min}) results in a higher peak. A lower coupling flattens the peak since the probability of overlap of independent step stimuli is lowered.

V. COHERENCE RESONANCE

If we let the FN system be driven purely by a noise term as opposed to the sum of sinusoidal and noise terms (as in SR), then the system can still tune to an optimal noise intensity at which the firings are most coherent. That is, at the optimal noise intensity, the characteristic correlation time of the sequence of firings is maximum [27] (rate of decay of correlations is slowest). This effect is called coherence resonance. CR has been analysed and predicted by the FN model using the standard Langevin approximation for the state variable (w) [27]. Intuitively, the CR effect can be traced to the existence of two different characteristic times in the FN system: the activation time t_a (time required to elicit firing) and the excursion time t_e (duration of action potential). Depending on the noise intensity, one of these two times dominates the average pulse duration (defined as the inter-spike interval). Thus, for small values of noise intensity, $t_a \gg t_e$ and for large values of noise intensities, $t_a \ll t_e$. When the noise intensity is large enough ($t_a \ll t_e$) so that excitations are frequent while at the same time fluctuations in the excursion time are low (high coherence), we get the observed CR effect. To quantify CR, the coefficient of variation (CV) of the interspike intervals is typically used. That is, we first compute the sequence of firings $\{t_i\}$ of a long spike train and from it, the interspike intervals $\{T_i\}$ where $T_i = t_i - t_{i-1}$. The coefficient of variation

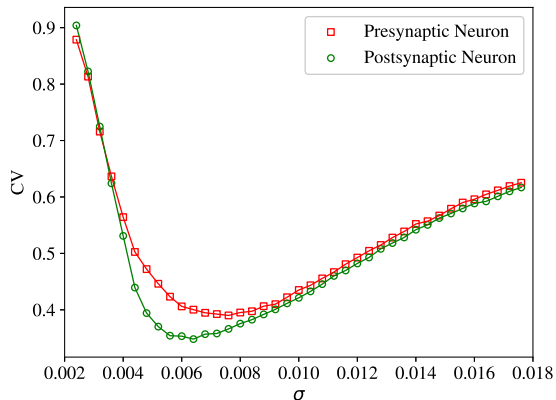


FIG. 6: Coefficient of variation as a function of standard deviation of noise for presynaptic and postsynaptic neurons. The simulations for each were run for 1000s and an ensemble average over 30 trajectories was taken to compute CV . For the postsynaptic neuron, $N = 3$ and $N_{\min} = 1$.

is defined as:

$$CV = \frac{\sqrt{\langle T^2 - \langle T \rangle^2 \rangle}}{\langle T \rangle} \quad (10)$$

The CR effect manifests as a minimum in the graph of CV versus noise intensity. Fig. 6 shows this for a presynaptic and postsynaptic neuron. At low and high noise intensities, both the presynaptic and postsynaptic neuron behave similarly while there is a marked difference in the approach to the minimum of CV (point of coherence resonance). The postsynaptic neuron hits the point of coherence resonance sharply in relation to the presynaptic case. Also, the minimum of CV occurs at a lower noise intensity when compared to the presynaptic neuron. This can be explained by the fact that at lower noise intensities, multiple independent stimuli from the synapses compensate for the low number of noise induced firings by the postsynaptic neuron alone. For $N_{\min} = 1$, each presynaptic firing elicits a postsynaptic action potential with high probability (barring rare noise induced failures). In the CR regime for the presynaptic neurons ($t_a \ll t_e$), the same noise intensity results in a lower activation time for the postsynaptic neuron (due to stimulation in addition to noise induced firings) while nearly coherent presynaptic excitations maintain the fluctuations in the postsynaptic spikes sufficiently low. In this sense, the postsynaptic neuron is better at exhibiting coherent firings in the CR regime. Decreasing the coupling by increasing N_{\min} on the other hand should raise the minimum of CV as well as shift the minimum to the right. To compensate this would require a higher number of synaptic inputs (N). At any rate, since both the presynaptic and postsynaptic neurons are exposed to the same noise intensity, the postsynaptic neuron is at least as good as the presynaptic neuron at coherent responses. For negligibly low noise intensities, $CV \approx 1$ which corresponds to Pois-

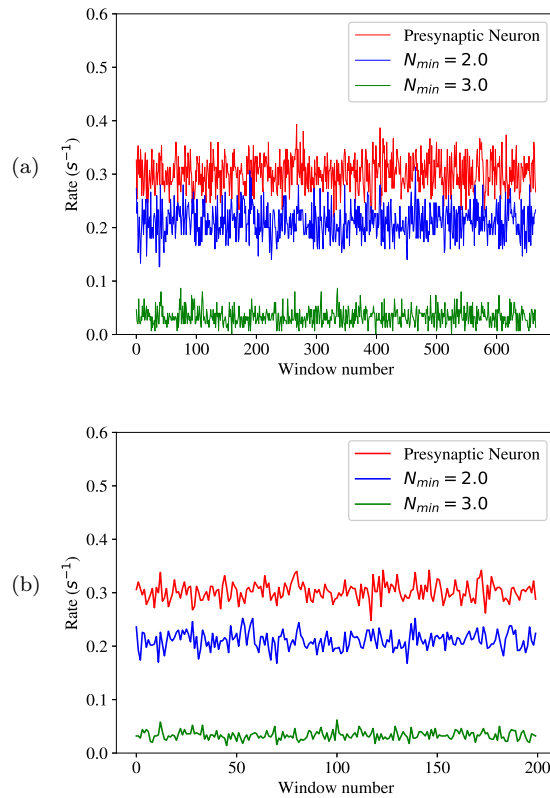


FIG. 7: Rate plots for presynaptic and postsynaptic neurons. All trajectories were simulated for 100000s. Rate plots in for the presynaptic neuron in (a) and (b) have been shifted up by 0.1 for ease of display. The postsynaptic neuron was setup with 20 inputs and is noiseless. The noise intensity was set at $\sigma = 0.003$ for the presynaptic neuron. The averaging window used to construct the rate plots is of length 150s for (a) and 500s for (b).

sonian statistics for the activation time [27]. Sharp departures from Poissonian statistics for spontaneous noise induced firings is therefore a hallmark of both higher synaptic inputs as well as a strong coupling.

VI. RATE AND INTER-SPIKE VARIABILITY

Sensory neurons are known to exhibit long term correlations in fluctuations of their spiking rates [28]. Graphically, this manifests as a fractal time series in the rate plot. The rate plot is calculated by choosing a time window of length T and computing the average rate of firing within that window for the whole spike train. Typical recordings from sensory nerves such as auditory neurons are known to exhibit widely fluctuating rates even when the averaging window length is significantly increased. Such scale-free rate fluctuations are quantified with standard fractal analysis tools such as Hurst exponents, detrended fluctuation analysis, etc. Rate fluctuations from a typical simulation are shown in Fig. 7. The magni-

tude of rate fluctuations (standard deviation) decreases slowly for fractal rates when compared to their nonfractal counterparts [29]. This can be shown by observing a power law relationship in periodograms and Fano factor time curves for the rate plots [28, 29]. A preliminary investigation of the same for the FN neurons by plotting Fano factor curves showed no significant fractal behaviour over white noise. The postsynaptic neuron in Fig. 6 was set as noiseless since we intended to observe rate variability from purely synaptic stimuli. We performed the same experiment with a noisy postsynaptic neuron as well and the mean rate was increased significantly beyond the mean presynaptic firing rate. The fractal characteristics however were unchanged.

As mentioned in section 5, spikes generated by the FN neuron are distributed across low and high activation times. Within a specific regime of either high or low activation time for the postsynaptic neuron, rate fluctuations can be increased by manipulating N , N_{\min} and σ . However, this reduces the fluctuation in the other regime. For instance, at a given noise intensity and coupling, increasing the number of synapses increases the fluctuation in lower activation times but reduces the fluctuation in higher activation times. To compensate, σ can be lowered to accommodate longer interspike intervals but that reciprocally affects the shorter interspike intervals as well. In other words, the fractal nature of rate fluctuations is limited in the synaptic FN model driven purely by white noise.

Besides rate fluctuations, variability in inter-spike times is another metric that has been shown to correlate with distinct pathological states in heart and gait dynamics [30]. The standard tool used to characterise inter-spike variability is detrended fluctuation analysis (DFA) which measures the fractal nature of a time-series [31]. Typically, DFA is performed on the inter-spike interval plot (defined in section 5). Briefly, the steps in the DFA algorithm are as follows:

First, the time series $x(t)$ is shifted by the mean and integrated (converted into a cumulative sum). Then, the series is divided into equal segments/boxes (overlapping or non-overlapping) of a given length and a least-squares line is fitted into each box. Finally, the RMS deviation between the data points and the least-squares fit is computed. The whole exercise is repeated for a range of box lengths. For a given box length l , the RMS fluctuation is computed as:

$$F(l) = \sqrt{\frac{1}{n} \sum_{i=1}^n (X_i - Y_i)^2} \quad (11)$$

where X_i is the integrated time series of length n and Y_i is the value of the least-squares fit. A double-logarithmic plot of $F(l)$ versus l reveals a linear increase and the slope α (via a linear fit) gives the degree of fractal behaviour of the time-series. For white noise, $\alpha \approx 0.5$ and for $\frac{1}{f}$ noise, $\alpha \approx 1.0$. We performed DFA on the inter-spike interval time series generated by pre and postsynaptic neurons.

No significant deviation from white noise character was observed for post-synaptic neurons for different values of coupling (N_{\min}). The DFA plots from representative simulations are shown in Fig. 8. For all simulations we performed, the DFA exponent α was between 0.4 and 0.6. These deviations are random artefacts of net negative and positive correlations respectively above the expected (uncorrelated) white noise firing pattern. We performed the simulations in Fig. 8 for higher noise intensities as well ($\sigma = 0.006$) and no qualitative difference was observed except a general lowering of mean RMS fluctuation (due to lower activation times). In general, a lower coupling allows for higher RMS fluctuations ($F(l)$). Depending on whether the postsynaptic neuron is exposed to lower or higher internal noise, the RMS fluctuations can be higher or lower in relation to presynaptic neurons (as exemplified in the contrast between Figs. 8(a) and 8(b)).

VII. CONCLUSIONS

We have introduced a minimal model for synaptic integration based on the excitation threshold (canard transition) of the Fitzhugh-Nagumo system. The model supports spatial summation and a modified version of temporal summation with an overall coupling that can be tuned to generate different mean firing rates for the postsynaptic neuron. We have then briefly investigated the postsynaptic neuron for the noise enhanced properties of stochastic and coherence resonance. The point of maximum synchronization with a driving signal was found to occur earlier for the postsynaptic case. Sensory information transmission in neurons is based on a rate code (stimulus strength encoded in terms of firing rate) to a major extent. Thus, reliable transmission of an external sinusoidal stimulus can be achieved for a postsynaptic FN neuron with many synapses and high coupling at a lower noise intensity than for peripheral neurons. For purely noise induced firings, postsynaptic neurons were seen to be more coherent than presynaptic ones, with maximum coherence achieved at a lower noise intensity. Different classes of neurons have different spontaneous mean firing rates (in the absence of strong stimuli). A further point of exploration could be to compare this rate with the mean rate predicted by the coherence resonance minimum. The rate fluctuations of the postsynaptic neuron in our model exhibit a small degree of self-affinity but insufficient in comparison with recordings of sensory neurons. An important exercise would be to replace white noise in the dynamical equations with coloured noise and observe the effect on postsynaptic firing statistics. For the simulations in this paper, we have considered only excitatory stimuli whereas neurons are stimulated by both excitatory and inhibitory synapses. This can be easily incorporated by adding a sign coefficient to the heaviside function in equation (5). The effect of manipulating the relative distribution of the two types of synapses on

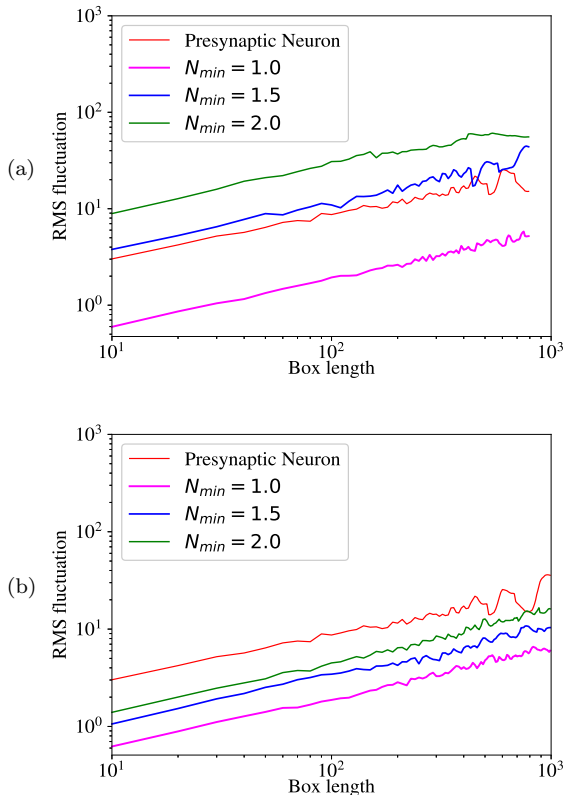


FIG. 8: Double-logarithmic plots of RMS fluctuation, $F(l)$ versus box length, l as defined by the DFA algorithm. A postsynaptic neuron was setup with 10 inputs. The noise intensity for presynaptic neurons in both (a) and (b) was set to $\sigma = 0.003$. In (a) the postsynaptic neuron is noiseless whereas in (b), it is noisy. Both simulations were run for 10000s. In (a) the postsynaptic neuron corresponding to $N_{\min} = 2.0$ generated < 1000 spikes so the maximum box length was limited to 800. In general, the RMS fluctuations for low coupling (greater N_{\min}) are greater than those for high coupling. Thus, the relative order of $F(l)$ in (a) follows $N_{\min} = 2.0 > N_{\min} = 1.5 > \text{Presynaptic neuron} > N_{\min} = 1.0$. In (b), since the postsynaptic neuron is noisy, internal noise induced firings superposed over synaptic excitations decrease $F(l)$ but the relative order among different values of N_{\min} is unchanged: Presynaptic neuron $> N_{\min} = 2.0 > N_{\min} = 1.5 > N_{\min} = 1.0$.

postsynaptic firing statistics is an interesting point of investigation. For our model, we have set the stable node away from the Hopf bifurcation point. However, setting the node close to the bifurcation point can reproduce certain important features of natural spiking activity such as mixed mode oscillations. The excitation threshold for the postsynaptic neuron in such a case will be defined by the canard explosion that occurs after the Hopf bifurcation. For chemical synapses, there is a non negligible delay between neurotransmitter release and postsynaptic firing. The step stimuli composing the postsynaptic input current in our model correspond to attenuated action potentials arriving from each dendrite. Our model therefore simulates the integration of stimuli *post* dendritic stimulation. The neurotransmitter mediated delay before dendritic stimulation can be modelled by adding delay terms to the time arguments of all presynaptic voltages. These delays need not be equal to each other and a distribution of delay times can serve as another interpretation of synaptic coupling.

-
- [1] A. L. Hodgkin and A. F. Huxley, *J. Physiol.* **117**, 500 (1952).
- [2] R. B. Stein, E. R. Gossen, and K. E. Jones, *Nat Rev Neurosci* **6**, 389 (2005).
- [3] A. Faisal, L. Selen, and D. Wolpert, *Nat Rev Neurosci* **9**, 292 (2008).
- [4] M. D. McDonnell and L. M. Ward, *Nat Rev Neurosci* **12**, 415 (2011).
- [5] A. Longtin, *J. Stat. Phys* **70**, 309 (1993).
- [6] J. J. Collins, C. C. Chow, and T. T. Imhoff, *Phys. Rev. E* **52**, R3321 (1995).
- [7] D. Nozaki and Y. Yamamoto, *Phys. Lett. A* **243**, 281 (1998).
- [8] B. Lidner and L. Schimansky-Geier, *Phys. Rev. E* **60**, 7270 (1999).
- [9] D. Valenti, G. Augello, and B. Spagnolo, *Eur. Phys. J. B* **65**, 443 (2008).
- [10] J. A. Acebrón, A. R. Bulsara, and W.-J. Rappel, *Phys. Rev. E* **69**, 026202 (2004).
- [11] E. N. Davidson, Z. Aminzare, B. Dey, and N. E. Leonard, *Chaos* **29**, 033105 (2019).
- [12] M. Desroches, M. Krupa, and S. Rodrigues, *J. Math. Biol* **67**, 989 (2013).

- [13] J. Mitry, M. McCarthy, N. Kopell, and M. Wechselberger, *J. Math. Neurosci* **3**, 12 (2013).
- [14] M. Diener, *The Mathematical Intelligencer* **6**, 38 (1984).
- [15] E. M. Izhikevich, *Dynamical systems in neuroscience: the geometry of excitability and bursting* (The MIT Press, 2007).
- [16] J. Durham and J. Moehlis, *Chaos* **18**, 015110 (2008).
- [17] N. Popovi, *J. Phys.:Conf. Ser.* **138**, 012020 (2008).
- [18] B. Alberts, A. Johnson, J. Lewis, D. Morgan, M. Raff, K. Roberts, and P. Walter, *Molecular Biology Of The Cell* (Garland Science, 2014).
- [19] E. R. Kandel, J. H. Schwartz, T. M. Jessell, S. A. Siegelbaum, and A. J. Hudspeth, *Principles Of Neural Science* (McGraw-Hill, 2013).
- [20] D. Purves, G. J. Augustine, D. Fitzpatrick, W. C. Hall, A. LaMantia, J. O. McNamara, and S. M. Williams, *Neuroscience* (Sinauer Associates, 2004).
- [21] P. E. Kloeden and E. Platen, *Numerical Solution of Stochastic Differential Equations* (Springer, New York, 1992).
- [22] H. C. Tuckwell and R. Rodriguez, *J. Comput. Neurosci* **5**, 91 (1998).
- [23] L. Gammaitoni, P. Hanggi, P. Jung, and F. Marchesoni, *Rev. Mod. Phys.* **70**, 223 (1998).
- [24] R. Rai and H. Singh, *Phys. Rev. E* **62**, 8804 (2000).
- [25] J. Douglass, L. Wilkens, E. Pantazelou, and F. Moss, *Nature* **365**, 337 (1993).
- [26] D. Russel, L. Wilkens, and F. Moss, *Nature* **402**, 291 (1999).
- [27] A. S. Pikovsky and J. Kurths, *Phys. Rev. Lett.* **78**, 775 (1997).
- [28] M. C. Teich, Fractal neuronal firing patterns, in *Single Neuron Computation* (Academic Press Professional, Inc., USA, 1992) p. 589.
- [29] S. B. Lowen, L. S. Liebovitch, and J. A. White, *Phys. Rev. E* **59**, 5970 (1999).
- [30] A. L. Goldberger, L. A. N. Amaral, J. M. Hausdorff, P. C. Ivanov, C.-K. Peng, and H. E. Stanley, *Proceedings of the National Academy of Sciences* **99**, 2466 (2002).
- [31] C.-K. Peng, S. V. Buldyrev, S. Havlin, M. Simons, H. E. Stanley, and A. L. Goldberger, *Phys. Rev. E* **49**, 1685 (1994).